Fall 9-2-2011

Forces at Individual Pseudopod-Filament Adhesive Contacts

Govind Paneru

Prem S. Thapa

Sean P. McBride
Marshall University, mcbrides@marshall.edu

David Moore-Nichols

Bruce M. Law

See next page for additional authors

Recommended Citation

Paneru G, Thapa P S, McBride S P, Nichols D M, Law B M and Flanders B N 2011 Forces at individual pseudopod-filament adhesive contacts. Appl. Phys. Lett. 99 093702

Authors
Govind Paneru, Prem S. Thapa, Sean P. McBride, David Moore-Nichols, Bruce M. Law, and Bret N. Flanders

AIP | Applied Physics Letters

Forces at individual pseudopod-filament adhesive contacts

Govind Paneru, Prem S. Thapa, Sean P. McBride, David Moore-Nichols, Bruce M. Law, and Bret N. Flanders

Citation: Applied Physics Letters **99**, 093702 (2011); doi: 10.1063/1.3628454
View online: http://dx.doi.org/10.1063/1.3628454
View Table of Contents: http://scitation.aip.org/content/aip/journal/apl/99/9?ver=pdfcov
Published by the AIP Publishing

Forces at individual pseudopod-filament adhesive contacts

Govind Paneru,[1] Prem S. Thapa,[1] Sean P. McBride,[1] David Moore-Nichols,[2] Bruce M. Law,[1] and Bret N. Flanders[1,a)]
[1]*Department of Physics, Kansas State University, Manhattan, Kansas 66506-2601, USA*
[2]*Imaging and Analytical Microscopy Lab, University of Kansas, Lawrence, Kansas 66045, USA*

(Received 1 June 2011; accepted 28 July 2011; published online 2 September 2011)

On-chip cellular force sensors are fabricated from cantilever poly(3,4-ethylene dioxythiophene) filaments that visibly deflect under forces exerted at individual pseudopod-filament adhesive contacts. The shape of the deflected filaments and their ~3 nN/μm spring constants are predicted by cantilever rod theory. Pulling forces exerted by *Dictyostelium discoideum* cells at these contacts are observed to reach ~20 nN without breaking the contact. © *2011 American Institute of Physics*. [doi:10.1063/1.3628454]

The forces that cells exert on substrates at adhesive contacts are critical to basic processes such as migration and cell division. Pseudopods are exploratory appendages that crawling cells like *Dictyostelium discoideum*, leukocytes,[1] and breast cancer cells[2] extend to probe the anterior substrate surface. Adhesive contact between the tips of the pseudopods and the substrate occurs frequently. These are the first contacts that the cell makes with the anterior substrate region. In addition to force-application, environmental sensing occurs at these contact sites, influencing whether the cell alters or persists in its direction-of-migration.[3] Despite the importance of pseudopod-substrate adhesive contacts in force transmission and environmental sensing, there has been little characterization of pseudopod-substrate adhesion at the single contact-level.

The most widely used technique for characterizing cellular forces is the deformable substrate method where cell-induced wrinkling or marker-displacement of the elastic substrate is observed.[4] A key advantage of this approach is that the substrate displacements occur in the imaging plane of the optical microscope, permitting direct visualization of the process. However, the forces at the discrete adhesive contact sites are not directly measured but are instead extracted by a non-trivial modeling effort that correlates the measured substrate displacement-field with the inferred force field and with the discrete sites.[5] Off-substrate forces may be directly measured with an atomic force microscope (AFM) with exquisite precision[6]; however, visualization during such measurements, which are usually made in a plane normal to the optical imaging plane, can be a challenge. Methodology for the simultaneous visualization and direct characterization of forces exerted by individual pseudopodia is needed.

To this end, we have fabricated on-chip cantilever poly(3,4-ethylene dioxythiophene) (PEDOT) filaments that visibly deflect under forces exerted at individual pseudopod-filament contacts. PEDOT was chosen for its biocompatibility.[7] A typical 3.2 μm long, ~400 nm wide pseudopod is indicated by the arrow in Figure 1(a). Direct characterization of an individual pseudopod requires a probe of comparable dimension. To produce such filaments, the simple polymerization technique *directed electrochemical nanowire assembly* (DENA) was employed.[8] Briefly, a 3 μl aliquot of aqueous solution containing 0.01 M 3,4-ethylene dioxythiophene and 0.02 M poly(sodium styrene sulfonate) was deposited across the ~30 μm gap between a pair of tapered, lithographic Au electrodes. The filament in Figure 1(b) was produced by applying a ±3.5 V 20 kHz square wave voltage signal across the electrodes to induce filament growth from the right electrode at a rate of ~5 μm/s. The voltage signal was terminated when the filament reached the desired length of ~14 μm. The scanning electron microscopy (SEM) based image in the inset shows its lengthwise-averaged width to be 320 ± 30 nm. Comparison to Figure 1(a) shows filament and pseudopod widths to be comparable, as desired. These filaments are rigidly bonded to the on-chip electrode but not to the glass substrate and, hence, are cantilever structures.

Type KAx3 *D. discoideum* cells were grown at 24 °C in Petri dishes containing HL-5 culturing medium.[9] Prior to transfer to the chips, 1000 μl of the cell-medium suspension was centrifuged for ~10 s at 1.34×10^3 g. The HL-5 supernatant was replaced with 1000 μl of 12 mM phosphate buffer, followed by gentle shaking for 1 min. This process was twice-repeated before suspending the cells in 300 μl of phosphate buffer and starving them for 4-6 h. To prevent evaporation of the cell medium, a 60 μl hybridization chamber (Grace Biolabs) was adhered to the filament-laden chip. Before sealing with a transparent lid, 10 μl volumes of cell suspension and phosphate buffer were deposited in the chamber. Typical cell surface densities were ~10^3 mm^{-2}. A waiting time of ~20 min following cell deposition was required for the cells to settle, to begin migrating, and for a single cell to randomly contact the filament.

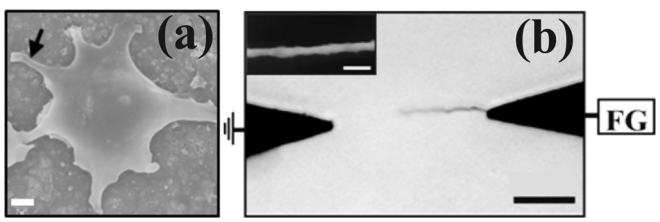

FIG. 1. (a) Scanning electron micrograph of fixed *D. discoideum* cell with extending pseudopods. Scale bar = 1 μm. (b) Optical micrograph of PEDOT filament grown by the DENA technique. FG ≡ function generator. Scale bar = 10 μm. Inset: a scanning electron micrograph of a filament. Scale bar = 1 μm.

a)Electronic mail: bret.flanders@phys.ksu.edu.

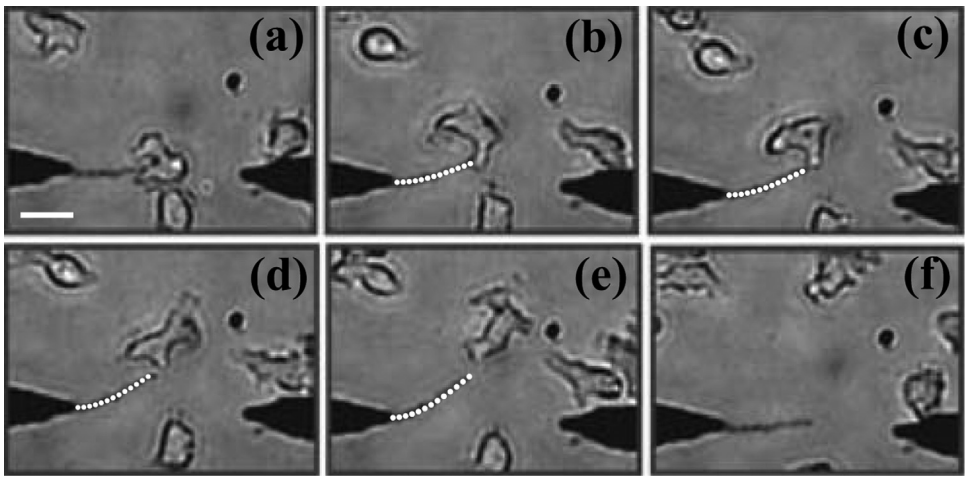

FIG. 2. Series of optical micrographs of a cantilever PEDOT filament (a) in its neutral position 7 s after contact initiation by the pseudopod. Scale bar = 10 μm; (b)-(e) while being deflected upwards by the cell at times 37 s, 46 s, 54 s, and 65 s, respectively; and (f) at time 105 s when the filament is back in its neutral position after release by the cell (where a video of this event is shown at 3 × the actual rate). The white dotted curves on panels (b)-(e) represent the deflected filament shapes predicted by cantilever rod theory (enhanced online) [URL: http://dx.doi.org/10.1063/1.3628454.1].

Figures 2(a)–2(f) constitute a series of bright-field images (collected on a microscope of 0.75 numerical aperture) of four *D. discoideum* cells migrating randomly on a glass slide. One of these cells contacts the cantilever filament in Figure 2(a). This cell deflects the filament by exerting pulling force on it in Figures 2(b)–2(e), and releases it in Figure 2(f) (see online video of this event, shown at 3 × the actual rate). The shape of the pseudopod evolves throughout this event. We have observed $\sim 10^2$ such events. Clearly, these filaments are flexible enough to deflect visibly upon contact by a foraging cell (yet stiff enough to resist visible thermal motion). In the small deflection approximation, the shape of a cantilever rod of length L and radius r that is bent by a force F_A applied to its free end is described by[10]

$$\delta_F(x) = \frac{F_A}{6EI} x^2(3L - x), \tag{1}$$

where $I = \pi r^4/4$ is the area moment of inertia of the solid cylindrical rod, E is Young's modulus of the rod-material, and x denotes position along the rod length with respect to the fixed end. This function was fitted to the deflected filament profiles in panels (b)–(e), as designated by the white dashed curves overlaid upon these micrographs. As discussed below, no adjustable parameters were used in achieving these fits.

Figure 3(a) shows a scanning electron micrograph of a *D. discoideum* cell that was fixed shortly (5 s) after establishing pseudopod-filament contact.[11] An enlarged view of the contact region is shown in Figure 3(b). The surface of the pseudopod-tip is butted against the left side of the filament. The pseudopod does not encompass the filament. The two other pseudopod-filament contacts that were characterized also exhibited butt-joint contact-structure. Deflection by a *pulling*-force (as illustrated in Figures 2(b)–2(e)) that is applied at a simple butt-joint implies *adhesive* contact between the joined pseudopod and filament surfaces. As with better characterized adhesive contacts like focal adhesions[12] and actin foci,[13] adhesion is likely due to numerous transmembrane cellular adhesion molecules (of undetermined type) that bind the substrate surface.

Knowledge of the radius, Young's modulus, and length of a solid, cylindrical cantilever rod permits calculation of its theoretical spring constant k_{Th} in the small deflection approximation: $k_{Th} = 3EI/L^3$.[10] To assess how well this simple equation predicts the spring constants of PEDOT filaments, we have used an AFM to directly measure the k_F values of several filaments and compared these values to the corresponding k_{Th} values. The AFM (MFP-3D, Asylum Research) was calibrated by pressing its cantilever (NP-0, Veeco) against a hard glass surface to quantify the cantilever deflection-photodiode voltage relationship. The spring constant k_C of this cantilever was determined by the thermal method.[14] Hooke's law then gives the magnitude of the elastic force exerted by the cantilever F_C for deflection δ_C: $F_C = k_C\delta_C$. To measure the spring constant of a PEDOT filament k_F, the AFM cantilever was pressed against an individual filament by lowering the AFM head by distance Δz, as depicted in Figure 4(a).[15] This measurement deflects the filament by distance δ_F and yields a δ_C vs Δz profile (solid line in Figure 4(b)). The opposing forces exerted by the filament F_F and cantilever F_C are equal in magnitude (Newton's 3rd law); hence, $k_F\delta_F = k_C\delta_C$, where δ_F is the (unknown) filament displacement and $F_F = k_F\delta_F$. Δz is related to δ_C and δ_F by $\Delta z = \delta_C + \delta_F$, giving $k_F = k_C(\Delta z/\delta_C - 1)^{-1}$.

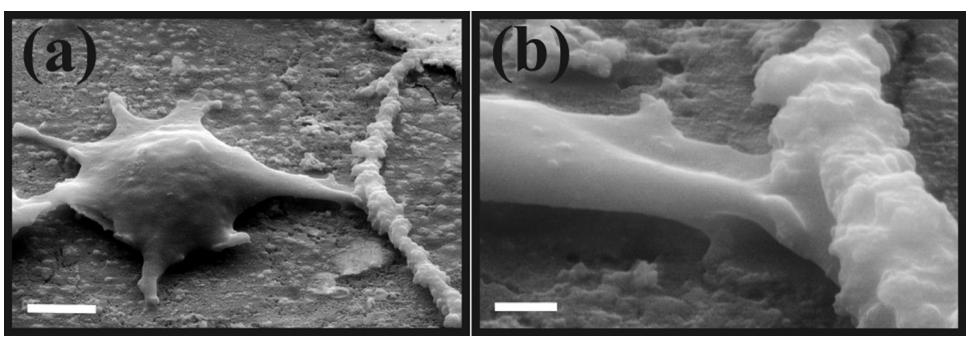

FIG. 3. (a) Scanning electron micrograph of fixed cell with a pseudopod in direct contact with PEDOT filament. Scale bar = 2 μm. (b) Enlarged view of contact region. Scale bar = 500 nm.

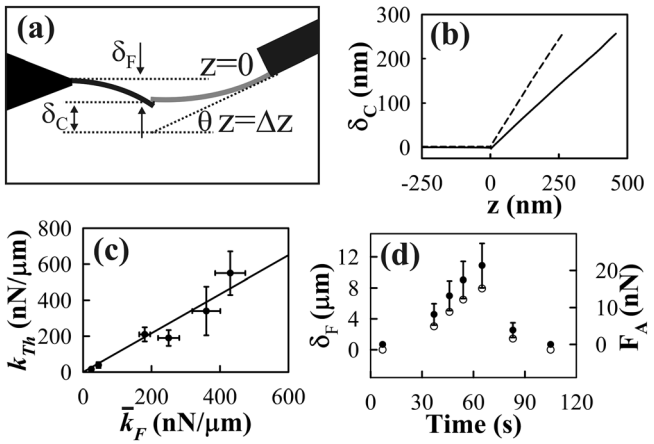

FIG. 4. (a) Schematic of AFM-based determination of the filament spring constant. The gray curve denotes the AFM cantilever while the black curve denotes the filament. (b) AFM cantilever deflection magnitude δ_C versus vertical position of AFM head z for pressure against a rigid surface (dashed profile) and a PEDOT filament (solid profile). (c) Plot of the theoretical spring constants of PEDOT filaments versus their measured spring constants. The solid line is the best linear fit to the points. (d) Cell enforced deflection (unfilled circles) and force (filled circles) measured during the event depicted in Figure 2.

The effects of AFM cantilever tilt by angle θ (11° for all cases in this study) and off-end loading of the filament are accounted for by corrective factors, yielding[16]

$$k_F = k_C(\Delta z/\delta_C - 1)^{-1}\left(\frac{L-\Delta L}{L}\right)^3 \cos^{-2}\theta. \qquad (2)$$

ΔL is the distance from the filament tip to the loading point as measured via an internal optical microscope in the AFM. The spring constants of six different PEDOT filaments k_F were obtained by substituting into Eq. (2) the corresponding k_C, L, ΔL, and $\delta_C/\Delta z$ values given in Table I. Each filament was characterized three times with each of three different cantilevers whose spring constants varied significantly. The averages of these nine determinations for each of the six filaments are reported in column $\bar{k}_F$.

To calculate the k_{Th} values, we approximate the PEDOT filament shapes as cylinders having radii equal to the lengthwise averaged radii of the filaments. These SEM determined values are reported with their standard deviations in Table I. Also, we have taken $E = 2.0$ GPa, the average of two recent determinations (1.8 GPa (Ref. 17) and 2.26 GPa (Ref. 18)) of the PEDOT Young's modulus. Figure 4(c) plots k_{Th} vs $\bar{k}_F$. The horizontal error bars denote the standard error associated with the $\bar{k}_F$ determinations; the vertical error bars result from propagation of radial standard deviations and ± 0.03 μm length nonuniformities in the k_{Th} calculations. The solid line, the best-fit to these points (constrained to pass through the origin), has a near-unity slope of 1.08. Hence, the correlation between k_{Th} and $\bar{k}_F$ is strong, indicating that cantilever rod theory provides reasonable predictions of the filament spring constants. While it lies beyond the scope of this letter to do so here, the PEDOT filaments have lengthwise radial variations of 10%–20%, so the success of $k_{Th} = 3EI/L^3$ deserves further examination.

Figure 4(d) shows the filament deflection-values (unfilled circles) corresponding to frames 2(a)–2(f) (except for the point at 83 s whose image is not shown in Figure 2).

TABLE I. Measured properties of six PEDOT filaments and their associated spring constants (in units of nN/μm).

r (μm)	L (μm)	ΔL (μm)	$\frac{\delta_c}{\Delta z}$	k_c	k_{Th}	k_F	$\bar{k}_F$
0.72 ± 0.08	13.24	1.3	0.59	450	550	490	430
0.64 ± 0.06	15.55	2.2	0.49	270	210	170	180
0.52 ± 0.06	12.18	1.8	0.77	110	190	240	250
0.61 ± 0.12	12.38	0.5	0.57	310	340	380	360
0.28 ± 0.06	12.04	2.2	0.42	58	16	20	24
0.29 ± 0.06	9.50	0.5	0.90	55	39	40	45

SEM analysis of this filament revealed a 220 nm lengthwise averaged radius and 16.0 μm length. Hence, as demonstrated above, cantilever rod theory ($k_F = 3EI/L^3$) indicates a spring constant k_F of 2.7 ± 0.7 nN/μm; the sizable uncertainty is expected given the highly nonlinear functionality of k_F. Conversion of these δ_F-values to F_A-values via Hooke's law ($F_A = \delta_F k_F$) yields the filled circles in Figure 4(d). (The error bars reflect the propagated uncertainties of δ_F and k_F.) As these data and Figure 2(e) show, F_A reaches 21 nN without breaking contact. The measured force values of 8, 13, 18, and 21 nN reported in Figure 4(d) (along with $I = 1.8 \times 10^{-27}$ m^4 and $E = 2.0$ GPa) were used to calculate the parameters $F_A/6EI$ in Eq. (1) to fully determine the shape functions (white dotted lines) shown in Figures 2(b)–2(e), respectively. The close agreement with the measured shapes confirms the usefulness of cantilever rod theory for predicting the elastic properties of these PEDOT filaments. In future studies, we will employ this methodology for the simultaneous visualization and measurement of forces exerted at single pseudopod-filament contacts to articulate the factors that dictate adhesion strength and duration.

This work was partially supported by National Science Foundation grants PHY-0646966 (B.N.F.) and DMR-0603144 (B.M.L.).

[1]P. Friedl, S. Borgmann, and E. B. Brocker, J. Leukoc. Biol. **70**, 491 (2001).
[2]A. Muller, B. Homey, H. Soto, N. F. Ge, D. Catron, M. E. Buchanan, T. McClanahan, E. Murphy, W. Yuan, S. N. Wagner, J. L. Barrera, A. Mohar, E. Verastegui, and A. Zlotnik, Nature **410**(6824), 50 (2001).
[3]N. Andrew and R. H. Insall, Nat. Cell Biol. **9**(2), 193 (2007).
[4]A. K. Harris, D. Stopak, and P. Wild, Science **208**, 177 (1980).
[5]U. S. Schwartz, N. Q. Balaban, D. Riveline, A. Bershadsky, B. Geiger, and S. A. Safran, Biophys. J. **83**, 1380 (2002).
[6]G. Pfister, C. M. Stroh, H. Perschinka, M. Kind, M. Knoflach, P. Hinterdorfer, and G. Wick, J. Cell Sci. **118**(8), 1587 (2005).
[7]S. M. Richardson-Burns, J. L. Hendricks, and D. C. Martin, J. Neural Eng. **4**, L6 (2007).
[8]P. S. Thapa, B. J. Ackerson, D. R. Grischkowsky, and B. N. Flanders, Nanotechnology **20**, 235307 (2009).
[9]D. J. Watts and J. M. Ashworth, Biochem. J. **119**, 171 (1970).
[10]L. D. Landau and E. M. Lifshitz, *Theory of Elasticity* (Butterworth-Heinemann, Oxford, 2000).
[11]J. A. Araujo, F. C. Téran, R. A. Oliveira, E. A. A. Nour, M. A. P. Montenegro, J. R. Campos, and R. F. Vazoller, J. Electron Microsc. **52**(4), 429 (2003).
[12]B. Geiger, J. P. Spatz, and A. D. Bershadsky, Nat. Rev. Mol. Cell Biol. **10**, 21 (2009).
[13]K. S. K. Uchida and S. Yumura, J. Cell Sci. **117**, 1443 (2004).
[14]J. L. Hutter and J. Bechhoefer, Rev. Sci. Instrum. **64**, 1868 (1993).
[15]S. Yang and T. Saif, Rev. Sci. Instrum. **76**, 044301 (2005).
[16]R. S. Gates and M. G. Reitsma, Rev. Sci. Instrum. **78**, 086101 (2007).
[17]H. Okuzaki and M. Ishihara, Macromol. Rapid Commun. **24**, 261 (2003).
[18]D. Tahk, H. H. Lee, and D. Y. Khang, Macromolecules **42**, 7079 (2009).